FIGURE 2.1

Conformations produced by rotation about C_2-C_3 bond of *n*-butane molecule. Each carbon atom in this molecule, being sp^3 hybridized, is tertrahedral with bond angles of 109.50°. The *planar cis* conformation, corresponding to the closest approach of the two bulky methyl groups, is the least stable. Conversely, the *planar trans* conformation, where the bulky groups are farthest apart, is the most stable. (After Young and Lovell, 1990.)

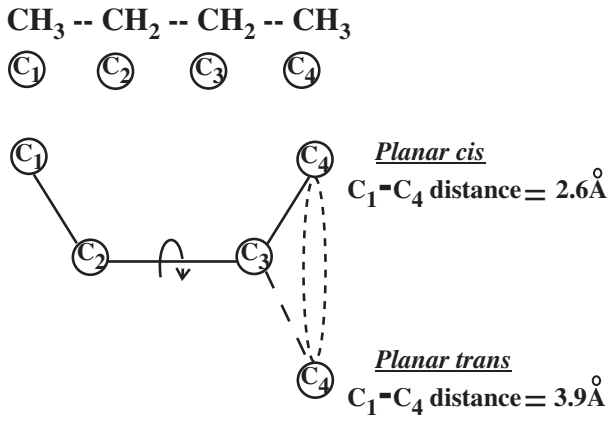

FIGURE 2.2

Newman and "saw horse" projections for *n*-butane. (a) A staggered state (planar *trans*) with angle of bond rotation $\varphi = 0$ and (b) an eclipsed state (planar *cis*) with $\varphi = 180°$.

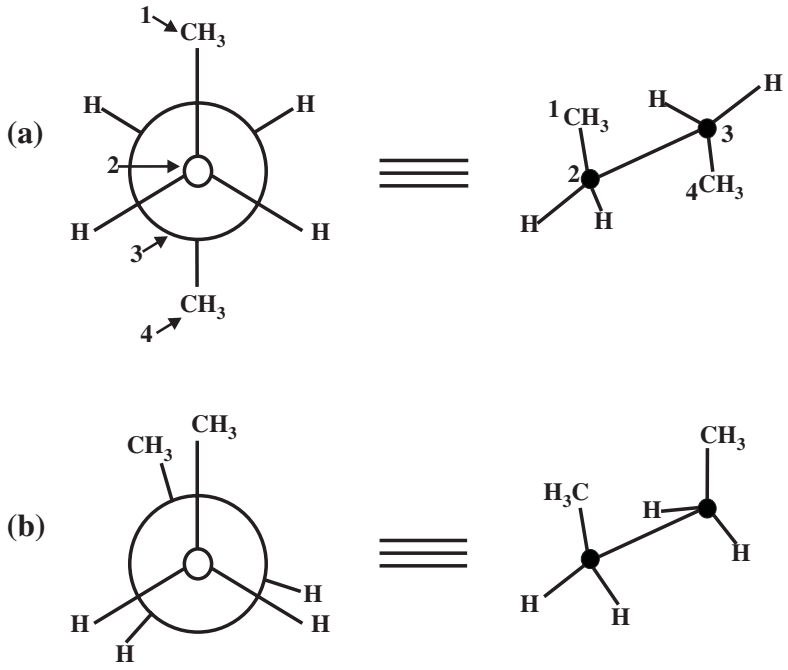

FIGURE 2.3

Potential energy of *n*-butane as a function of the angle of bond rotation. (After Young and Lovell, 1990.)

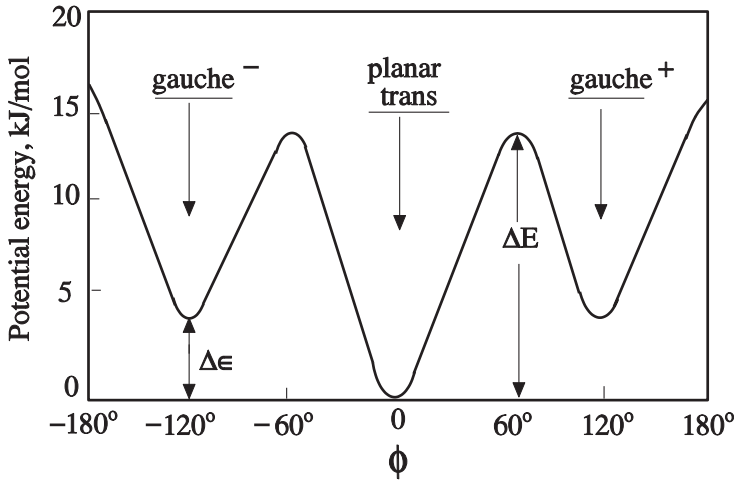

FIGURE 2.4

Newman projections of the eclipsed and staggered conformations of *n*-butane molecule. (After Young and Lovell, 1990.)

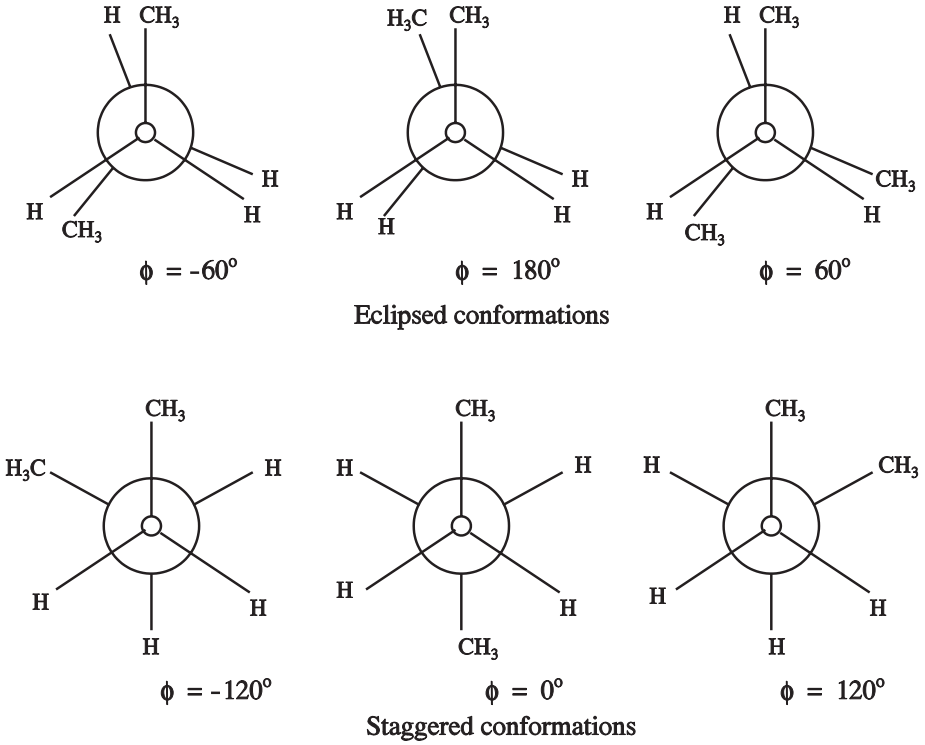

FIGURE 2.5

(a) Schematic diagram showing two adjacent carbons, C_n and C_{n+1}, in the main chain of polyisobutylene. (b) Newman projections of staggered conformations of adjacent carbons in the main chain.

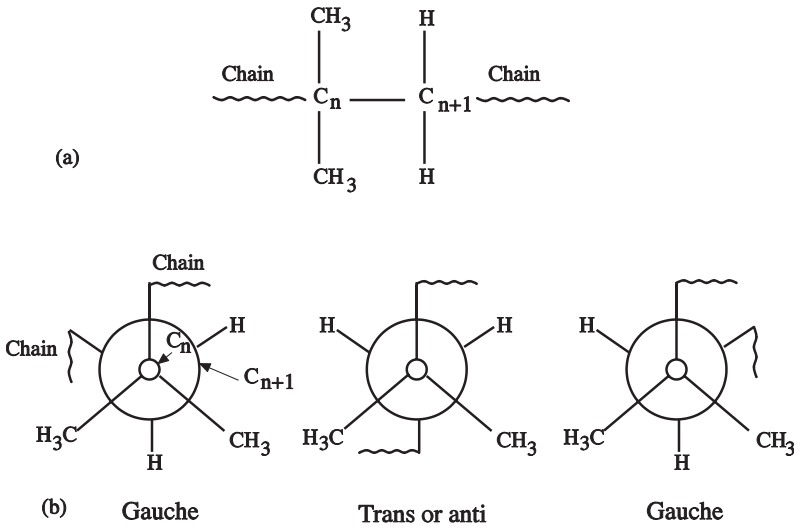

FIGURE 2.6

Newman projections of the six possible conformations of polypropylene.

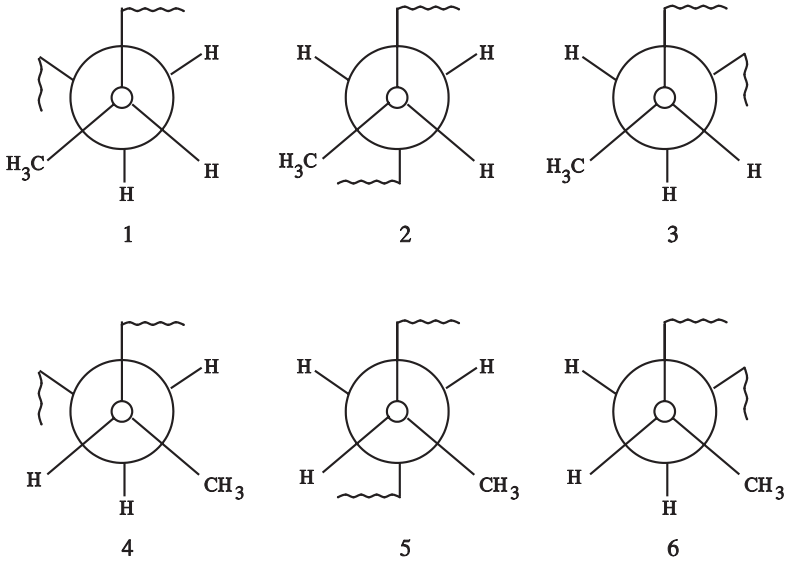

FIGURE 2.7

Model of the packing of polymer chains in the crystal structure of polyethylene in which a = 7.41 Å, b = 4.94 Å, and successive pendant atoms are 2.55 Å apart along the chain axis.

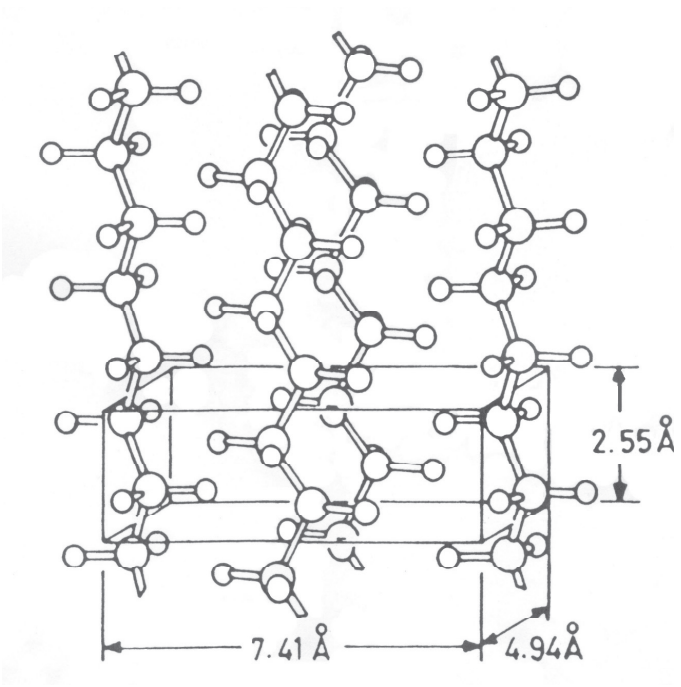

FIGURE 2.8

(a) Hydrogen bonds between neighboring chains of polyamide. (b) Alignment of chains in hydrogen-bonded sheets in the crystal structure of nylon-6,6. (After Holmes et al., 1955.)

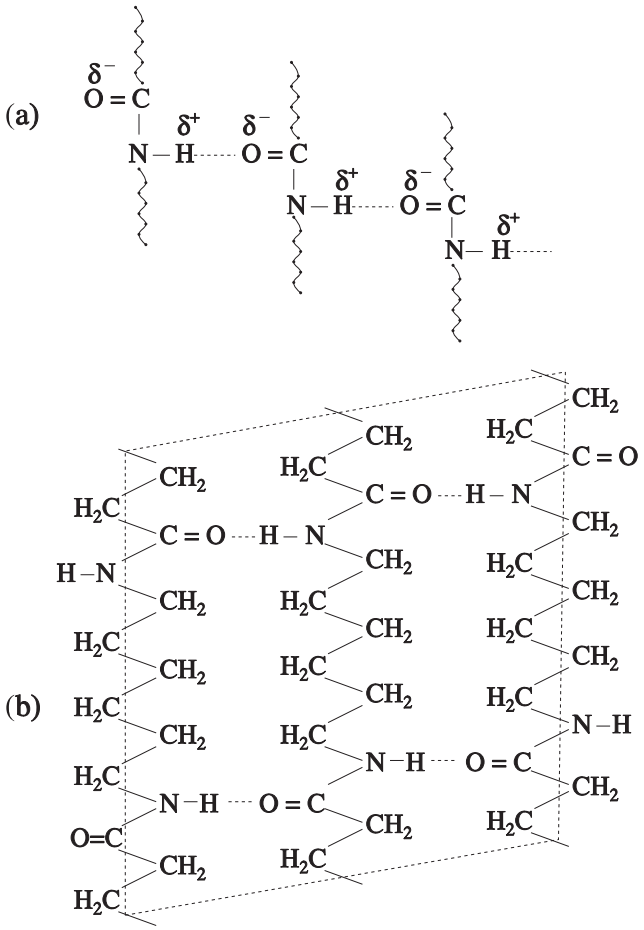

FIGURE 2.9

Skeletal representation of polyethylene chain in planar zigzag form.

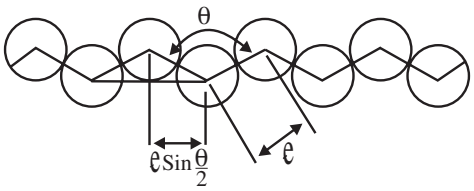

FIGURE 2.10

Schematic representation of a coiled polymer chain showing the end-to-end distance.

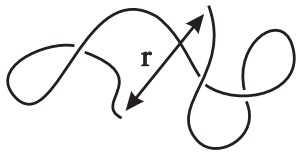

FIGURE 2.11

Diagrams of (a) isotactic, (b) syndiotactic, and (c) atactic configurations of $-(CH_2\text{-}CXY\text{-})_n-$ polymer. The corresponding Fisher projections are shown on the right.

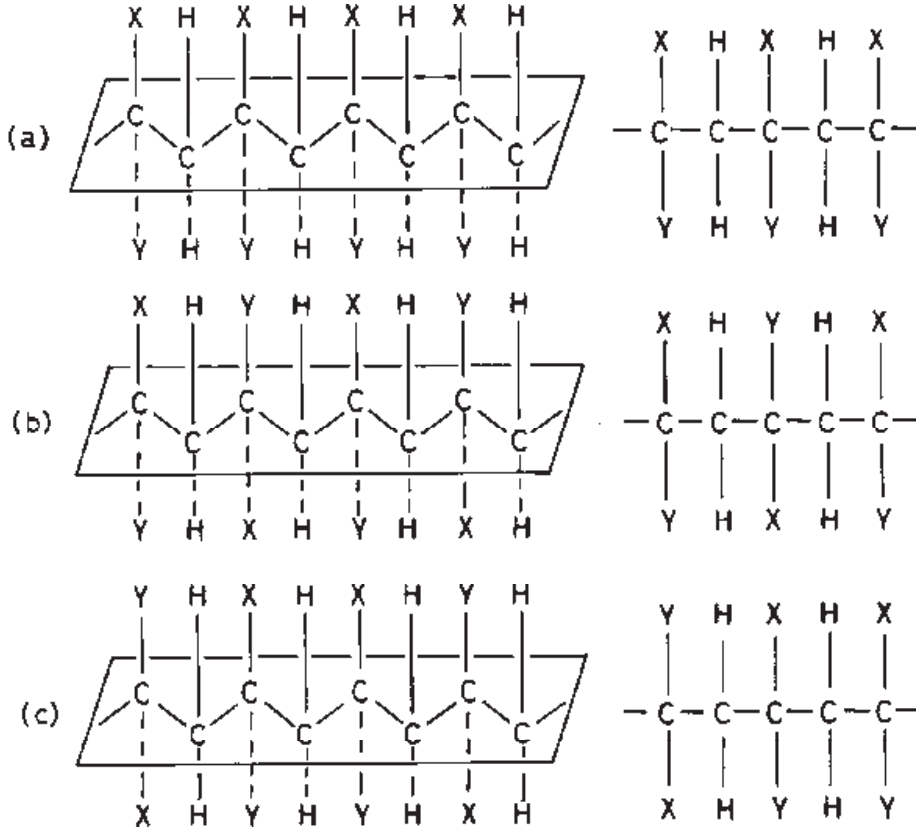

FIGURE 2.12

The probabilities (or fractions) of isotactic (*mm*), heterotactic (*mr*), and syndiotactic (*rr*) triads as a function of P_m, the probability of isotactic monomer placement during propagation. (Bovey and Tiers, 1960.)

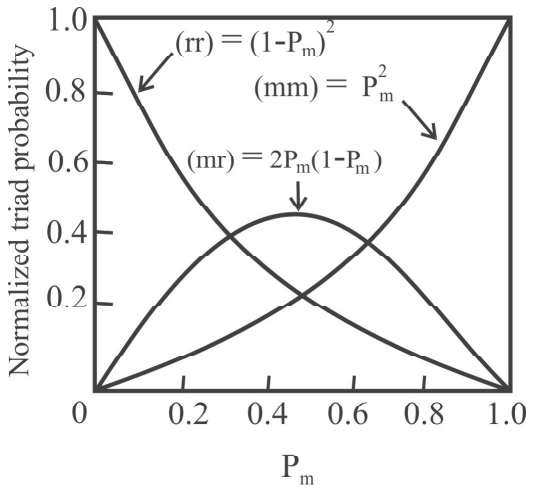

FIGURE 2.13

NMR spectra of poly(methyl methacrylate) (15% solution in chloroform, r = tetramethyl silane reference peak). (a) Mainly syndiotactic; (b) mainly isotactic. The methyl ester group appears at 6.40τ in both spectra and is unchanged by chain configuration. (Bovey, 1969.)

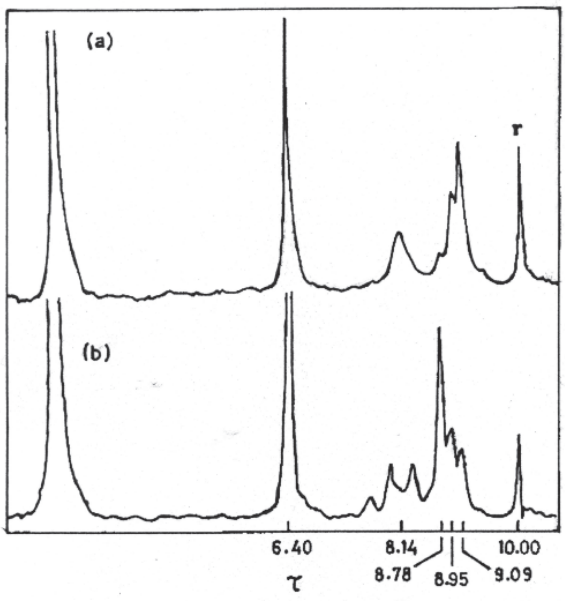

FIGURE 2.14

Isotactic, syndiotactic, and heterotactic triad configurations for poly(methyl methacrylate).

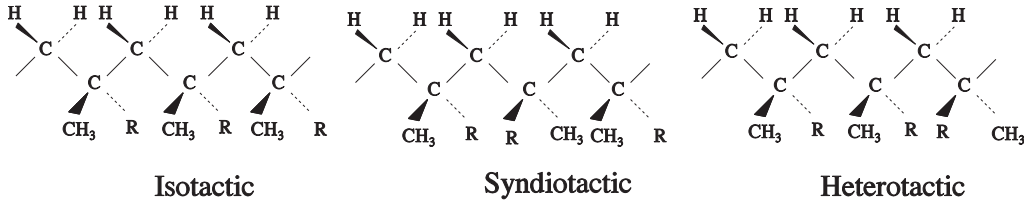

FIGURE 2.15

Test of Bernoullian model with data for polymer 1 and polymer 2 of Problem 2.13.

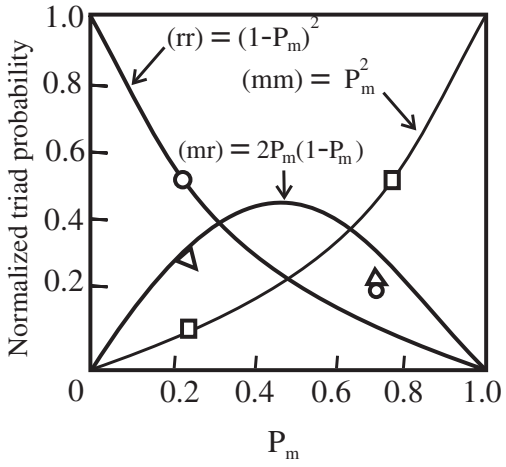

FIGURE 2.16

A typical WAXS curve for semicrystalline polyethylene where the intensity of scattering is plotted against diffraction angle 2θ. The amorphous hump is shown shaded.

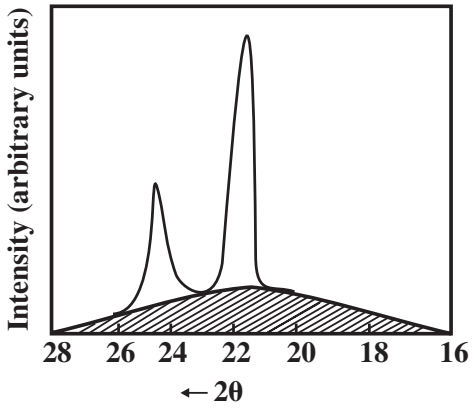

FIGURE 2.17

Schematic representation of (a) fold plane showing regular chain folding, (b) ideal stacking of lamellar crystals, (c) interlamellar amorphous model, and (d) fringed micelle model of randomly distributed crystallites.

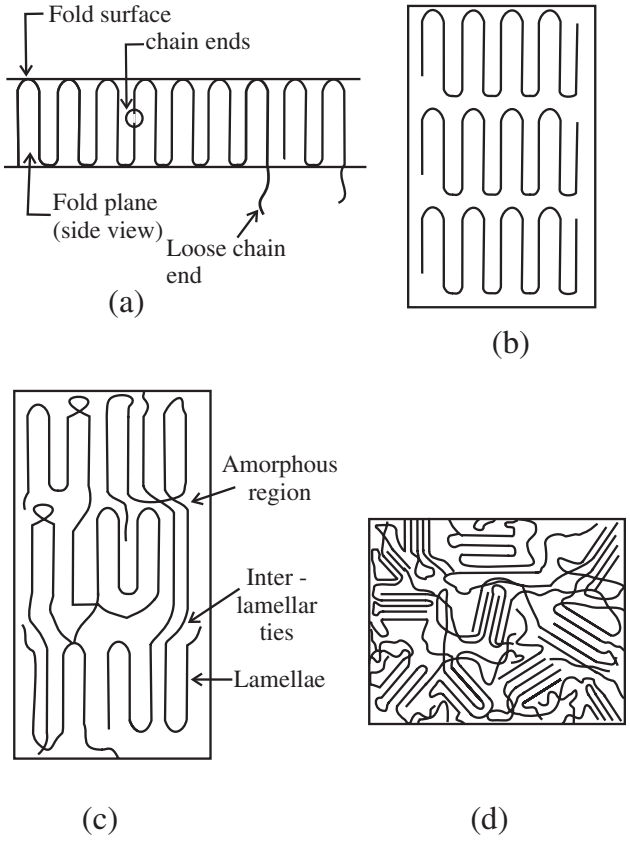

FIGURE 2.18

Spherulites in a siliconelike polymer, observed in the optical microscope between crossed polarizer. The large and small spherulites were grown by crystallization at different temperatures. (Adapted from Price, 1958.)

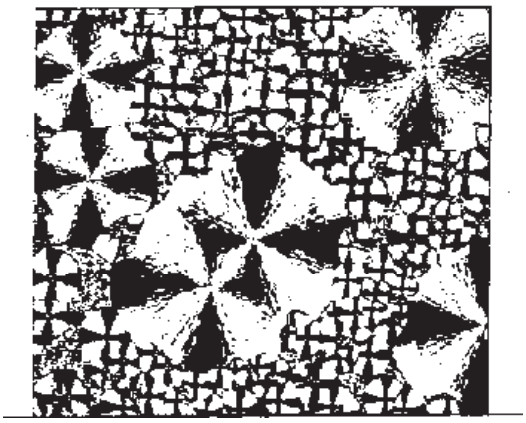

FIGURE 2.19

Schematic representation of the changes of specific volume of a polymer with temperature for (a) a completely amorphous sample (A–B–C), (b) a semicrystalline sample (A–D–E), and (c) a perfectly crystalline material (A–F–G).

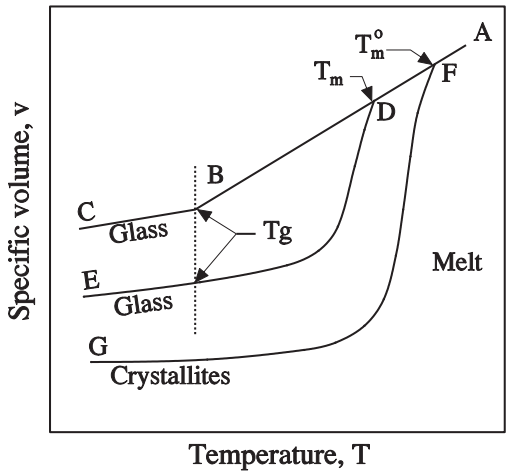

FIGURE 2.20

Schematic representations of volume (V) and enthalpy (H) variations with temperature. Also shown are variations with temperature of the volume coefficient of expansion (α) and the heat capacity (C_p), which are, respectively, the first derivatives of V and H with respect to temperature (T).

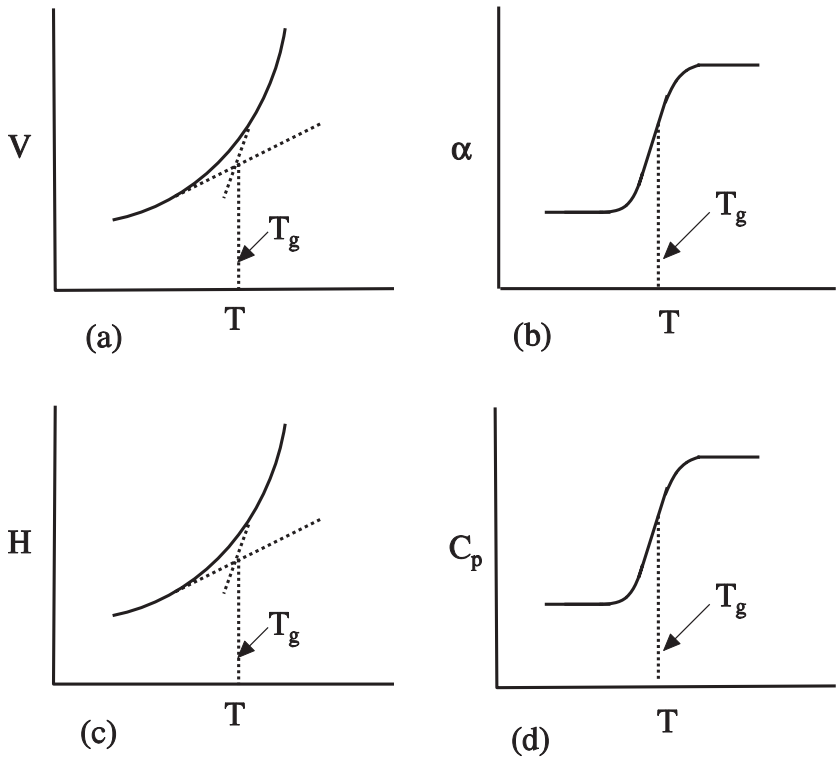

FIGURE 2.21

Five regions of viscoelastic behavior for a linear, amorphous polymer: I (a to b), II (b to c), III (c to d), IV (d to e), and V (e to f). Dotted line (···) shows the effect of crystallinity and dashed line (– – – –) that of crosslinking. (After Sperling, 1986.)

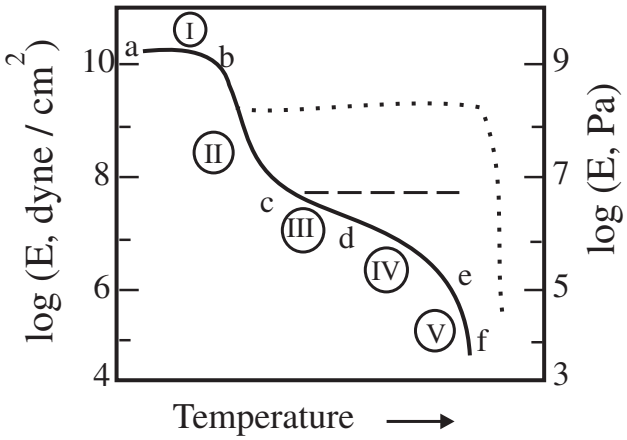

FIGURE 2.22

A quasicrystalline lattice of molecules (circles) exhibiting vacancies or holes. The arrow indicates molecular motion.

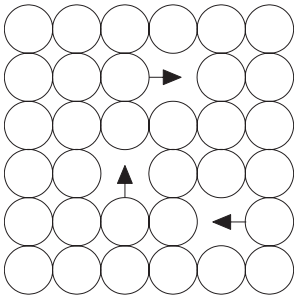

FIGURE 2.23

(a) Schematic representation of the variation of specific volume with temperature. The free volume (shaded area) is assumed to be constant at $v_f^\star$ below T_g and to increase as the temperature is raised above T_g. (b) Schematic illustration of free volume (Simha and Boyer, 1962).

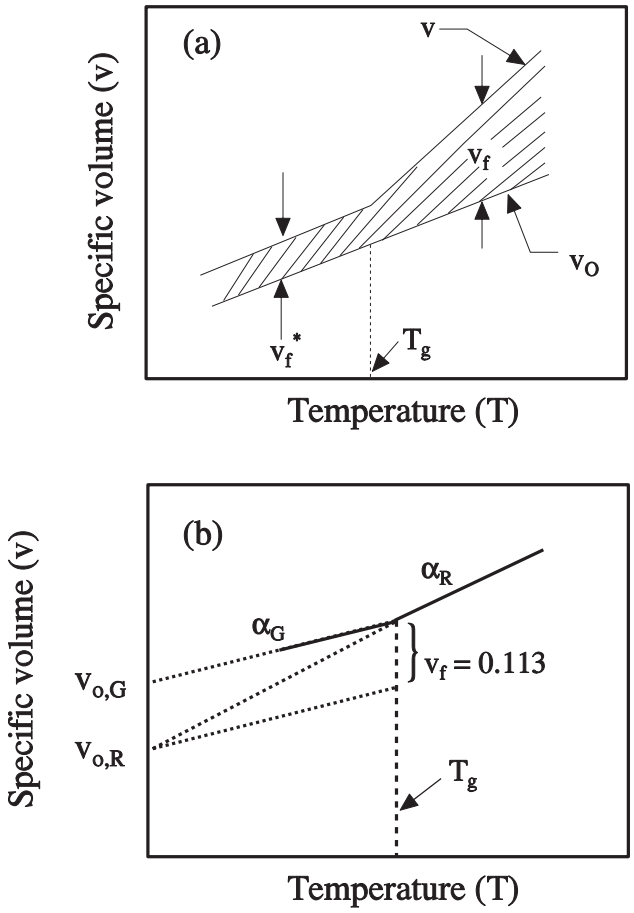

FIGURE 2.24

Plot of T_g against reciprocal molecular weight (data of Problem 2.29).

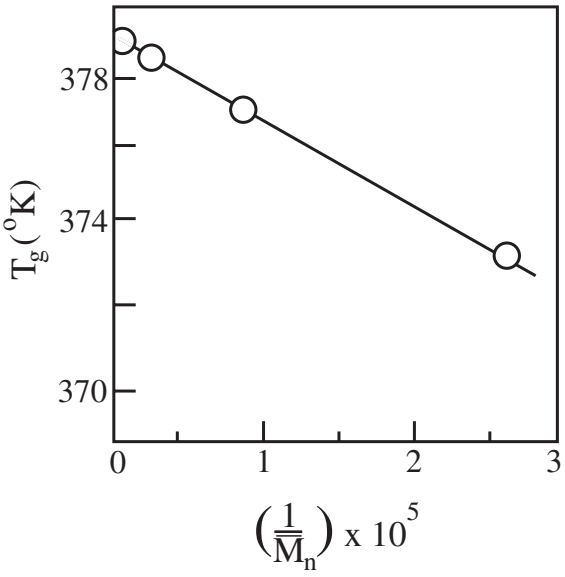

FIGURE 2.25

Plot of T_g against composition for PPO/PS blends according to (a) the linear equation, (b) the Fox equation, and (c) the Wood equation. Circles represent experimental points (data of Problem 2.32).

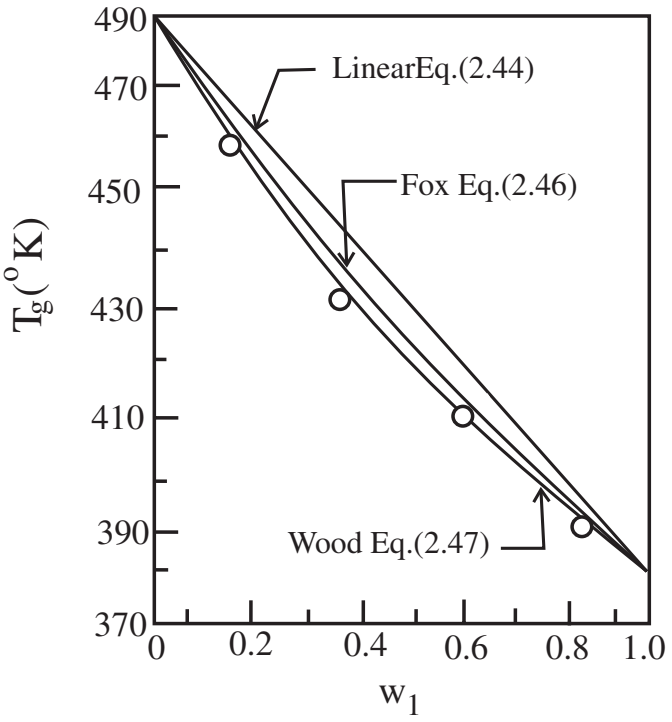

FIGURE 2.26

Plot of melt viscosity versus chain length Z for polyisobutylene fractions at 217°C. (After Fox and Flory, 1951.)

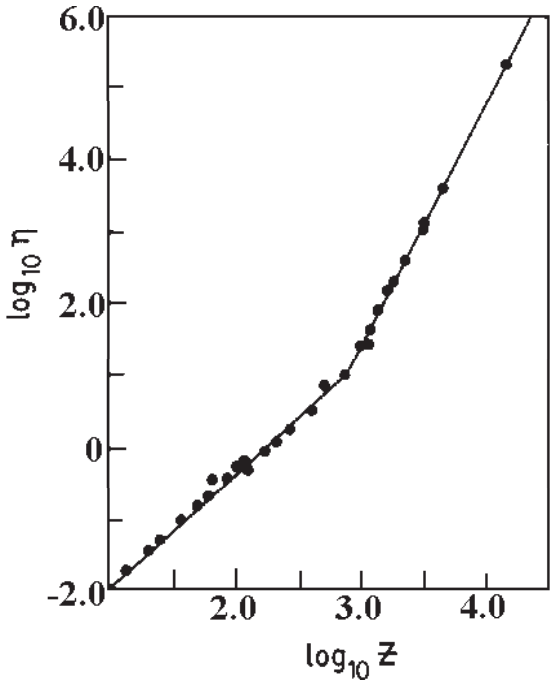

FIGURE 2.27

A model for reptation. The polymer chain moves among fixed obstacles, but cannot cross any of them. (After De Gennes, 1971; Sperling, 1986.)

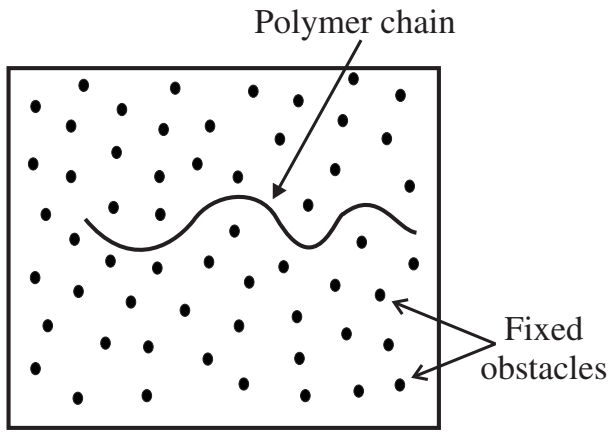

FIGURE 2.28

(a) Schematic representation of a polymer chain confined in a hypothetical tube contoured by fixed obstacles. (b) Movement of a "kink" along the chain. (After Cowie, 1991.)

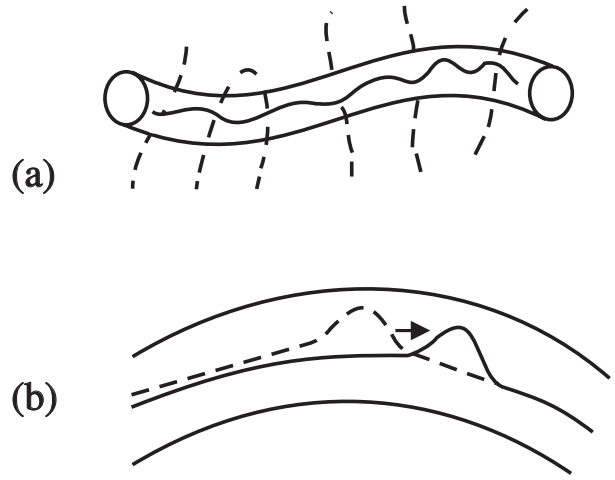

FIGURE 2.29

An analysis of the thermodynamic equation of state [Eq. (2.69)] for rubber elasticity using a general experimental curve of force versus temperature at constant length. The tangent to the curve at T is extended back to 0°K. For an ideal elastomer, the quantity $(\partial U/\partial \ell)_T$ is zero, and the tangent goes through the origin. The experimental line is, however, straight in the ideal case. (After Flory, 1953.)

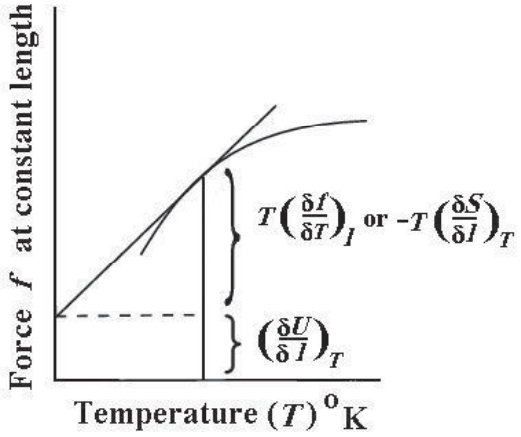

FIGURE 2.30

Idealized network structure of a crosslinked polymer. • indicates a crosslink (junction) and → signifies continuation of the network structure. Wavy lines between crosslinks are active network chain segments. (Note that for a tetrafunctional cross-link, as shown here, the number of crosslinks is one-half the number of active network chain segments.)

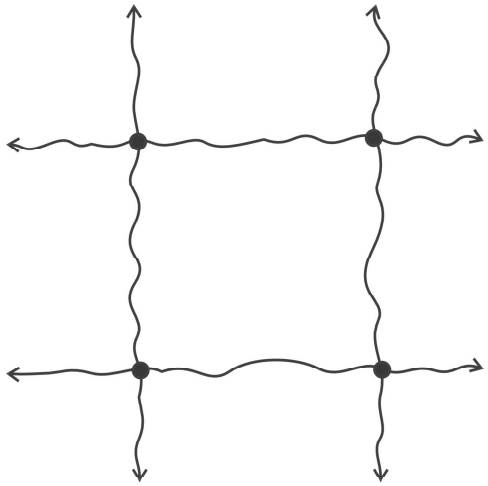

FIGURE 2.31

A Mooney-Rivlin plot with the data of Problem 2.42. (After Sperling, 1986.)

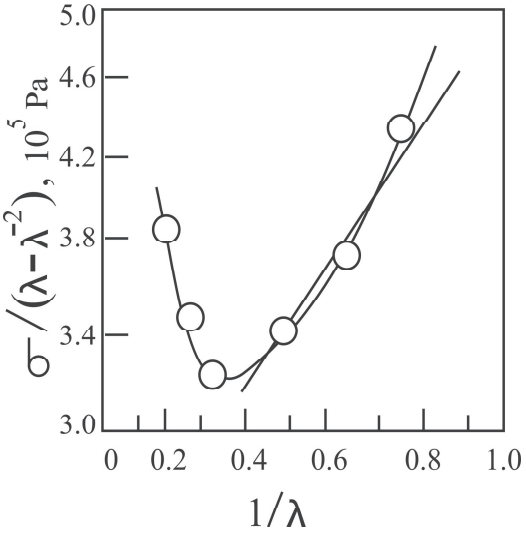

FIGURE 2.32

(a) Effect of ends of molecules on network structure. (b) Network structure and defects: • cross-links; ∘ terminus of a molecule; (1) elastically active chain; (2) inactive loop; (3) inactive loose end. An arrow (→) signifies continuation of the network structure. (After Flory, 1944.)

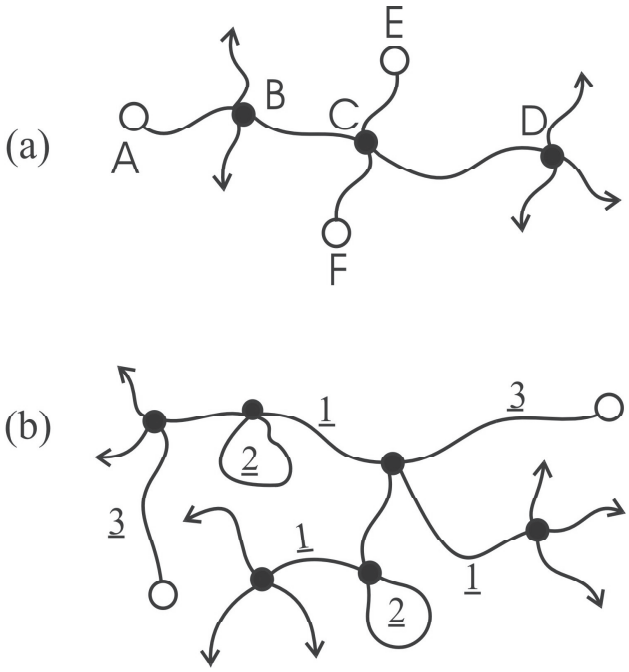

FIGURE A2.1

(a) Schematic representation of a coiled polymer molecule showing the end-to-end distance. (b) Diagram showing a coiled polymer molecule of end-to-end distance *r* in a rectangular coordinate system with one chain end fixed at the origin. (After Young and Lovell, 1990.)